Journal of King Saud University – Science 33 (2021) 101341

Contents lists available at ScienceDirect

Journal of King Saud University – Science

journal homepage: www.sciencedirect.com

Original article

Elemental composition and physical characteristics of the massive meteorite of the Saudi empty quarter

M.S. AlSalhi [a,b,*], V. Masilamani [b], Nasser Alarifi [c], W. Aslam Farooq [a,b], M. Atif [a,b,*], Shahid Ramay [a], Hayat Saeed Althobaiti [a], Saqib Anwar [d], Ibrahim Elkhedr [c], Bassam A. Abuamarah [c]

[a] Physics and Astronomy Department, College of Science, King Saud University, Riyadh, Saudi Arabia
[b] Research Chair for Laser Diagnosis of Cancer, King Saud University, Riyadh, Saudi Arabia
[c] Department of Geology and Geophysics, College of Science King Saud University, Riyadh, Saudi Arabia
[d] Industrial Engineering Department, College of Engineering, King Saud University, P.O. Box 800, Riyadh 11421, Saudi Arabia

ARTICLE INFO

Article history:
Received 18 October 2020
Revised 7 January 2021
Accepted 7 January 2021
Available online 14 January 2021

Keywords:
Laser-induced break down spectroscopy (LIBS)
X-ray fluorescence (XRF)
Scanning electron microscope (SEM)
X-ray diffraction (XRD)
Modern analytical methods

ABSTRACT

The meteorite found in the Empty Quarter of Kingdom of Saudi Arabia (KSA) is the largest meteorite found in the KSA and has the shape of an irregular ellipsoid with semi-axes of 0.65 m, 0.38 m, and 0.27 m; a density of 6400 kg/m^3; and a mass of 2550 kg. It is a massive piece belonging to the category of iron–nickel meteorites, which is contained in only 5% of the total showers. The present report is on the Elemental composition and physical characteristics of the massive meteorite of the saudi empty quarter employing with laser-induced break down spectroscopy (LIBS), X-ray fluorescence (XRF), scanning electron microscope (SEM), x-ray diffraction (XRD) and energy-dispersive x-ray spectrophotometry (EDX).

Present study has indicated that the meteorite is composed of about 5% Ni, 91% Fe, 1.51% P, 0.3% Co, and a host of other elements, most of them appeared as oxides. The measured density of the meteorite is 6400 kg/m^3 and it is confirmed by the micro-hardness test that the meteorite is porous (approximately about 19%). Based on our investigation, it is very likely that this meteorite would have "escaped" from the belt around Mars and Jupiter and is unlikely from the moon or elsewhere. This could be the first such study, employing the advanced instruments mentioned above regarding massive Saudi meteorite.

1. Introduction

A meteorite is a solid piece of debris possibly from a comet, asteroid, or a meteoroid originating from the outer space. During their passage through earth's atmosphere, most meteorites burn up and become what is commonly known as "shooting stars," with only a few small pieces finally landing on the earth's surface. There are three broad categories of meteorites: stony (mostly silicate minerals), iron (mostly of iron and nickel), and stony-iron meteorite (a mix of above two categories). Among the three categories, the first one constitutes 94%, the second 5%, and the last one only 1% of all meteorites. A study of physical properties, such as elemental composition, mechanical characteristics, and morphological aspects, would offer insights into the physical mechanisms of planetary belts and interstellar space. This is one of the main objectives of manned and unmanned space missions. In this context, elemental composition analysis employing laser-induced breakdown spectroscopy (LIBS) has been a convenient and effective analytical technique, since remote sensing is possible only with LIBS (Clegg et al., 2009; Corrigan et al., 2009) and not with other techniques such as atomic absorption spectroscopy (AAS), Auger Electron Spectroscopy (AES), and Inductively Coupled Plasma (ICP), which are commonly used for testing terrestrial minerals. Recent and more advanced techniques such as XRF and EDX also need samples for analysis. Hence, most of the studies on the elemental composition of meteorites from different places have been conducted using LIBS, with single-pulse or double-pulse excitation, though occasionally EDX has also been employed (Harmon et al., 2013; Senesi, 2014; Tempesta and Agrosì, 2016).

* Corresponding authors at: Physics and Astronomy Department, College of Science, King Saud University, Riyadh, Saudi Arabia.
E-mail addresses: malsalhi@ksu.edu.sa (M.S. AlSalhi), muhatif@ksu.edu.sa (M. Atif).
Peer review under responsibility of King Saud University.

Production and hosting by Elsevier

https://doi.org/10.1016/j.jksus.2021.101341
1018-3647/

The last two decades have seen a lot of research activity on the development, advancement, and execution of laser-induced break down spectroscopy (LIBS) as a practical and effective analytical tool that can be used for the study of air, water, and solid materials (Clegg et al., 2009; Corrigan et al., 2009; Cremers and Radziemski, 2006; Hahn and Omenetto, 2012), as well as geo-materials (Harmon et al., 2013; Senesi, 2014; Tempesta and Agrosì, 2016).

The LIBS technique has a variety of applications in almost all fields of science and engineering (Farooq et al., 2013, 2012; Ramakrishnaiah et al., 2012; Sarfraz et al., 2013) because it can analyze any state of matter (Farooq et al., 2014; Sturm and Noll, 2003; Tawfik et al., 2015, 2013); it can also be used to study space objects like meteorites for its chemical analysis (Masilamani et al., 2019). Senesi et al. (2016) investigated Agoudal iron meteorite with double-pulse laser-induced breakdown spectroscopy (DP-LIBS) coupled with optical microscopy [18]. Their experimental results clearly indicate the characterization and quantitative analysis of Agoudal iron. Qualitative analysis recognized the presence of the following elements: Ca, Co, Fe, Ga, Li, and Ni in Agoudal iron.

The present study presents the results of the investigation of the elemental composition of the biggest iron meteorite found in the kingdom of Saudi Arabia. Of the 36 recorded samples of meteorite, it is the largest meteorite found in KSA, discovered in the Ash Shargiah region in 1863, and its shape is that of an irregular ellipsoid with semi-axes of 0.65 m, 0.38 m, and 0.27 m; a density of 6400 kg/m^3; and a mass of approximately 2550 kg (see Fig. 1(a) and (b)). It is only 10 times lighter than the world's largest (25000 kg) meteorite found in Tanzania, and the next largest found in KSA is just a minion by comparison, just 0.936 kg. It has been classified as iron IIAB type from geological survey records. The elemental composition was found employing three independent analytical techniques—LIBS, XRF, and EDX. The study shows that the meteorite is iron-abundant, composed of 91% Fe, 5% Ni, 1.51% P, 0.3% Co, and a host of other elements. In addition, some important physical characteristics (mechanical, morphological, crystallographic properties) of the material, as measured by a host of analytical instruments, are also presented to gain insights into its origin.

Fig. 1. Photograph of the massive meteorite (ellipsoid with semi-axes of 0.65 m, 0.38 m, and 0.27 m), density of 6400 kg/m^3, and mass of approximately 2550 kg. This massive meteorite is placed in the College of Science, King Saud University, Riyadh.

2. Experimental

Small portions of this rather unique celestial object have been sawn off and put under investigation. The instruments used were LIBS (Applied Spectra, USA), XRF (S8 Tiger, Brucker), EDX, and SEM (JSM-6380 LA, JEOL).

For LIBS, a laser beam with wavelength 266 nm serving frequency 10 Hz, pulse width 10 ns and peak power 10 MW. The laser beam was focused on the sample size 2 cm × 2 cm with a spot area 0.5 mm^2 on the sample to produce excitation and ionization of the elements and compounds present in the sample. The characteristic discrete atomic lines (excited and ionized to different levels) and the continuous band of plasma (due to recombination of free electrons with the ions) were captured and focused onto a spectrograph (consisting of a grating and charge-coupled device), so that the relative proportion of different elements present in the focal spot of the sample could be displayed with a personal computer (PC) monitor.

XRF employs x-rays from Rh (Max voltage of 60 kV) at a wavelength of 1.54 × 10^{-9} nm as the excitation source (instead of 1064 nm Nd:YAG laser). This high-energy photon produces excitation and ionization of the elements in the sample. Since the inner electrons are excited, the resultant emission (called x-ray induced fluorescence) is a characteristic emission of very short wavelength, which is sometimes accompanied by Auger electrons. Both techniques LIBS and XRF are being used for elemental analysis but they differ in the principle of diagnosis.

Such characteristic x-ray elemental lines could be obtained by exciting the atoms by bombardment with electron beams available in SEM (used commonly for surface morphological analysis) as well. It is important to note that all the LIBS lines occur in the visible region of 400–800 nm, and the detector is a charge-coupled device (CCD) camera. However, in XRF and EDX, the emission is in the 1–5 nm regions, and a suitable crystal (such as Thallium for the XRF) is required.

The other sophisticated instruments employed are the Ultima IV for XRD; SEM (JSM-6380 LA, JEOL), S8 Tiger, Brucker for XRF.

3. Results and discussion

In the beginning of the universe, only particles and gaseous matter were enriched. When they were separated from each other because of the Big Bang explosion, they started cooling and forming clumps, on account of gravitational and celestial forces. When these clumps collided among themselves, melted, and re-cooled, cosmic dust formed. Some of these evolved at different stages of time and environments, coalescing to become strong meteorites, iron-mild meteorites, or a combination of both. In any case, these meteorites are about 700 million years older than the rocks on earth (Weisberg et al., 2006).

3.1. LIBS analysis

LIBS spectra of the meteorite sample were taken at different positions and with different laser energies, delay times, and gate widths in air. The optimized LIBS spectrum was taken at 5 millijoule laser energy, 1 micro-second delay, and 10 micro-second gate widths. Each spectrum was an average of 15 shots taken at three different positions of the sample. The LIBS spectrum is shown in Fig. 2 and was analyzed with the software provided by Applied Spectra with the LIBS instrument. We have found that iron is in highest abundance in the sample with Ni and P in different proportions (See Table 1). The prominent lines of the iron observed in the spectrum are given in Table 2. These lines have also been confirmed from the National Institute of Standards and Technology

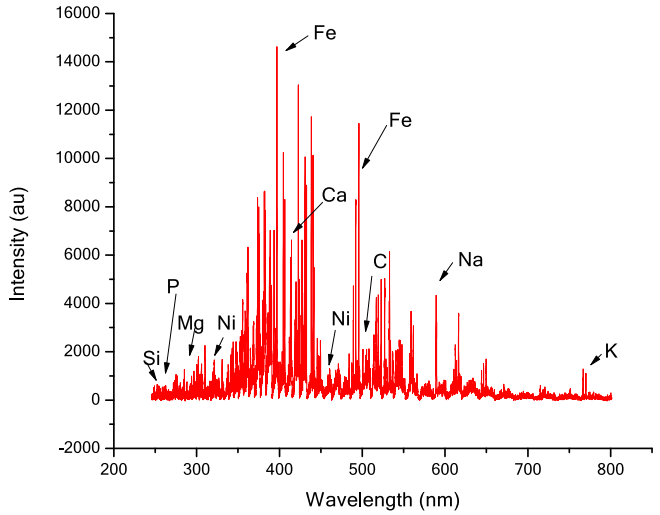

Fig. 2. Laser (266 nm YAG laser) induced breakdown spectra of the meteorite sample.

Table 1
Elemental abundance.

Element	LIBS %	XRF %	EDX %
Fe	9.5	91	94
Na	2.8	–	
K	6	–	
Mg	8	0.1	
Ca	1.6	0.3	
Ni	9	5	5.6
Mn	1.4	–	
P	–	1.5	
Si	–	0.4	

(NIST) database. Table 2 shows some of the most prominent lines of Fe.

The best way to estimate the elemental concentration with the LIBS technique is from calibration curves drawn for the corresponding elements (Abedin et al., 2011; De Giacomo et al., 2007; Dequaire et al., 2017; "Lpsc xlviii,", 2017; Senesi et al., 2016), because it is impossible to simulate an alloy of a meteorite; however, in the present case it is not possible to draw such calibration curves. Farooq et al. (2013) considered the integrated intensities of the strongest lines for each detected element of their sample as their abundance and carried out the quantitative analysis. Although, the method is not very precise, it can give approximate abundances for the constituents of the sample. We have adopted the same procedure to evaluate the percentage abundance of the elements present in the sample. The integrated intensities of the strongest lines in the present estimation are given in Table 3.

3.2. X-ray fluorescence analysis

Fig. 3 shows the characteristic x-ray lines of different elements present in the sample. Note that the sharp lines of different elements arise from different levels of excitation. For example, Fe Kα is due to x-ray emission when an electron of iron returns from the L (n = 2) to the K shell (n = 1) with an energy of 6.4 keV, resulting in a relative abundance of 5800 units; Ni Kb1 is the x-ray emission when an electron of the Ni atom proceeds from the M shell (n = 3) to the L shell (n = 2), producing an x-ray of energy 7.4 keV. Table 3 gives an exhaustive list of the elements present, from Fe (91%) to trace element Gallium (Ga), with a concentration of 50 ppm. Note also that all elements manifest themselves as oxides.

Fig. 4 shows the EDX spectra of the sample indicating an abundance of Fe about 16 times greater than Ni. It gives only rather a gross picture of elemental composition mostly because the high-energy electron from SEM could not penetrate the material. So, this analytical technique is not as illustrative as others. All other such elements and their abundance are shown in Table 1. It is important to note the following:

1. The meteorite sample contains 29 elements. The most abundant of these in decreasing order of abundance are: Fe, Ni, K, Si, Cu, Co, Ca, Al, S, Cl, Cr, Mg, Zn. Even trace elements with 50 ppm Ga_2O could be detected.
2. Most of them are oxides mostly because when the meteorite entered into the earth's atmosphere with high velocity as a result of the gravitational pull, intense heat was generated so that almost every element got oxidized.
3. The most reliable of these three appear to be XRF; but LIBS has the advantage of remote sensing most suitable for extra-terrestrial investigations. A comparison of the elemental composition retrieved by the three techniques for this meteorite is given in Table 1.

3.3. Physical characteristics

In the previous section, it has been made clear that this meteorite is an alloy (forged in some celestial foundry) and, hence, knowing the standard physical characteristics would be of significant value.

XRD is the optical analogue of a microscope, with the former giving structural insight at the nano-scale. The crystallographic structure of this alloy was found by XRD with the wavelength of the copper alpha line = 1.3 nm, working with an anode voltage of 40 kV and a current of 30 mA, and the detector was an Ultima IV goniometer with suitable scintillation counter.

The XRD of the sample (see Fig. 5) shows sharp peaks at 2θ = 44.75°, 65°, and 82°, all from Fe. Such a crystal has a cubic structure with a = b = c = 0.28664 nm, and all three angles alpha = beta = gamma = 90°. It belongs to the Im3m symmetry group. Apart from

Table 2
Prominent atomic lines of Fe.

NO.	Wavelength (nm)	Intensity (a.u.)	Wavelength (nm)	Intensity (a.u.)	$A_{kj}g_k$	E_k
1	361.971	7185	361.877	4685	5.05E + 08	35 611.625
2	374.49	16,899	373.713	8097	127,000,000	27 166.820
3	374.721	15,647	374.948	5986	687,000,000	34 039.516
4	375.923	19,453	375.823	5334	444,000,000	34 328.752
5	381.715	14,408	381.584	4219	784,000,000	38 175.355
6	382.186	20,613	382.043	4653	600,000,000	33 095.941
7	404.693	23,524	404.581	5026	776,000,000	36 686.176
8	430.949	26,620	430.79	4334	304,000,000	35 767.564
9	432.688	25,632	432.576	4697	361,000,000	36 079.372
10	438.492	18,811	438.354	5879	550,000,000	34 782.421

Table 3
Integrated intensities of the strongest lines from the present estimation.

Eval2 V2.5.500 Admin 28.02.2017 13:38:34

Measured on 28.02.2017 13:22:01
Sample measured by admin
Measurement method: Best Detection-He34mm

Fe2O3	NiO	P2O5	SiO2	CuO	CoO	CaO	Al2O3	SO3	Cl	Cr2O3
5793,6 KCps	197,7 KCps	7,3 KCps	1,2 KCps	22,0 KCps	52,0 KCps	6,4 KCps	0,4 KCps	1,5 KCps	2,1 KCps	7,1 KCps
90,9 %	5,04 %	1,54 %	0,447 %	0,444 %	0,309 %	0,301 %	0,237 %	0,160 %	0,139 %	0,114 %

MgO	ZnO	Gd2O3	Ho2O3	K2O	TiO2	MnO	GeO2	Ga2O3	Na2O	Rh
0,1 KCps	5,5 KCps	1,5 KCps	3,7 KCps	0,6 KCps	0,5 KCps	0,9 KCps	0,9 KCps	0,3 KCps	0,0 KCps	38,4 KCps
0,105 %	920 PPM	685 PPM	551 PPM	289 PPM	185 PPM	138 PPM	121 PPM	50,4 PPM	0,0 PPM	0,0 PPM

Ag	Sb2O3	Dy2O3	Er2O3	Yb2O3	Ta2O5	PbO	Intensity Scal	Compton	Tb4O7
0,1 KCps	0,4 KCps	11,8 KCps	33,9 KCps	6,0 KCps	0,5 KCps	0,2 KCps		38,4 KCps	9,9 KCps
0,0 PPM	0,0 PPM	0,0 PPM	0,0 PPM	0,0 PPM	0,0 PPM	0,0 PPM	1,378	56 %	0,0 PPM

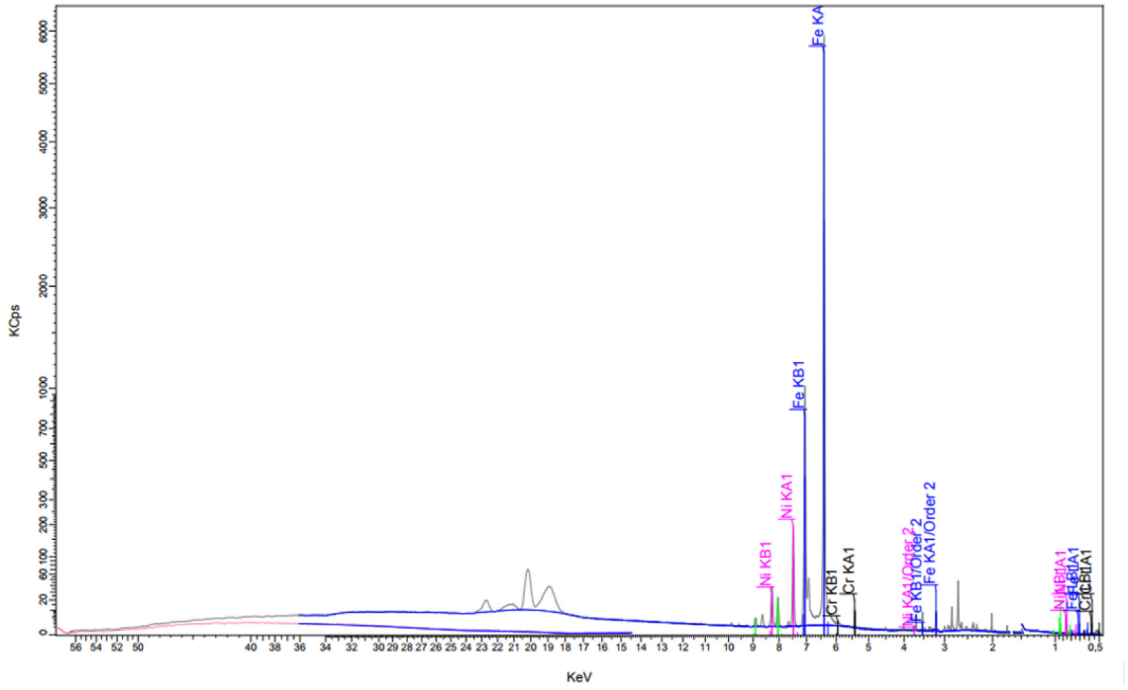

Fig. 3. XRF spectra of the above sample for elemental composition.

these, there are two more minor peaks at 43.5° and 51° due to the alloy of Fe and Ni with a ratio of 64% to 36%. This crystal also has a cubic structure but with a = b = c = 0.35922 nm.

Fig. 6 gives the scanning electron microscope (with 20 kV accelerating voltage to the electron) images of the surface at resolutions of (a) 100 μm, (b) 10 μm, and (c) 5 μm. The most important feature is that the specimen is riddled with potholes of smaller and larger radii, indicating a high degree of non-uniformity and porosity.

The above three results, namely XRD, SEM, and surface hardness, clearly indicate the surprising absence of martensite formation, despite the rapid heating and cooling that the sample could have experienced in rapid fall due to gravitation pull and also during its few million-year journey in the belt between Mars and Jupiter.

3.4. Major mineralogy

The above meteorite, sometimes called the "Al Khamasain meteorite," represents different mineral types as demonstrated by XRD and EDX. The study shows that the meteorite contains kamacite and dolomite. The kamacite α (Fe, Ni) occurred as the main essential metallic mineral constituent with other trace elements of an iron meteorite (Fig. 7). The notable trace elements are gallium (Ga), germanium (Ge), nickel (Ni), and chromium (Cr). The Ni concentration varies from 5 to 9%. All these trace elements and metallic minerals (concentration summarized in Table 3) were initiated and formed in a meteoritic environment. The meteorite had been formed as an alloy of Iron (Fe) and (Ni) in a proportion of either 90:10 or 95:5 (Table 4). The 5% or less Ni meteorite, often referred to as Octahedrites, cause the structure of the kamacite crystal to be isotropic and in cubic-crystal form. This structure only appears when the meteorite breaks along the crystal planes as bands, as shown in Fig. 8. These are very distinct with fine parallel straight lines seen across certain sections of the Octahedrite structure. These parallel lines are named after Johann G. Neumann (Hebbert, 1955). These lines suggest that the kamacite crystal's deformation is due to the shock induced during the impact events on the meteorite's parent body (Norton, 1994). In addition, these lines (lamellae) are approximately constant and reflect the cooling rate function, oriented along the planes. The

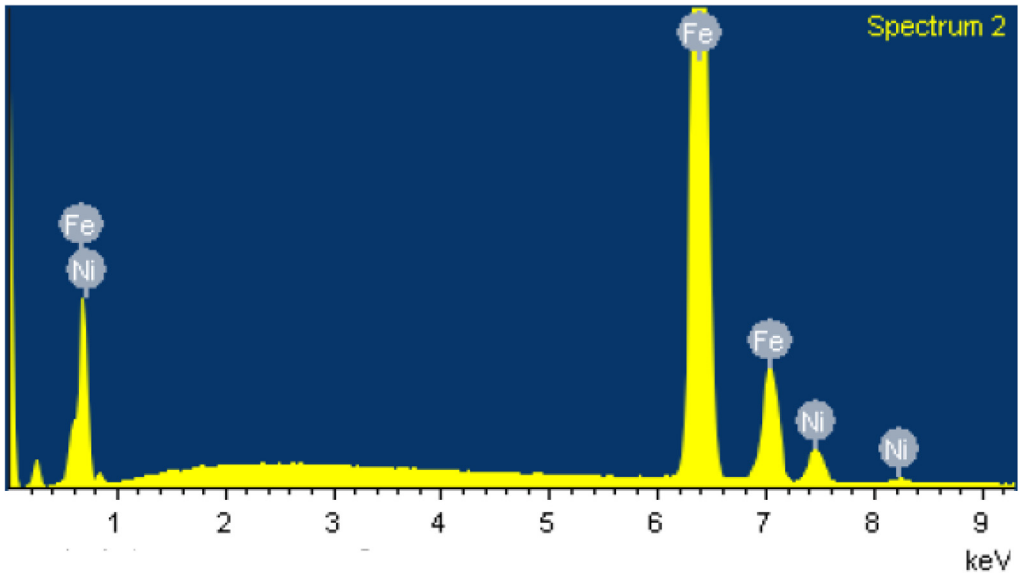

Fig. 4. EDX spectra of the sample.

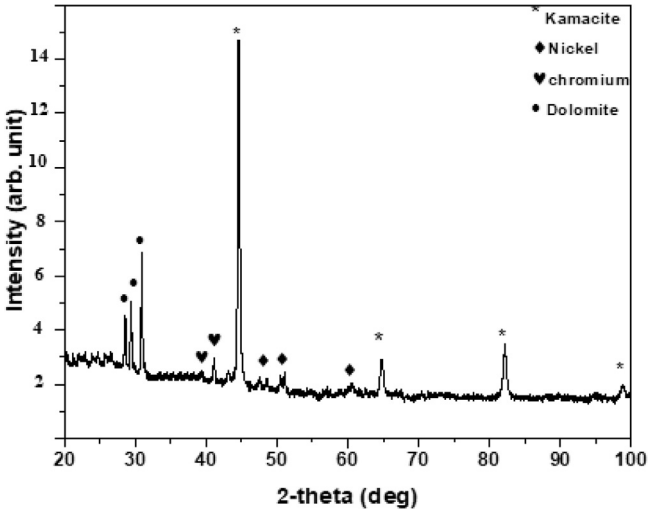

Fig. 5. XRD of the sample for crystalline determination.

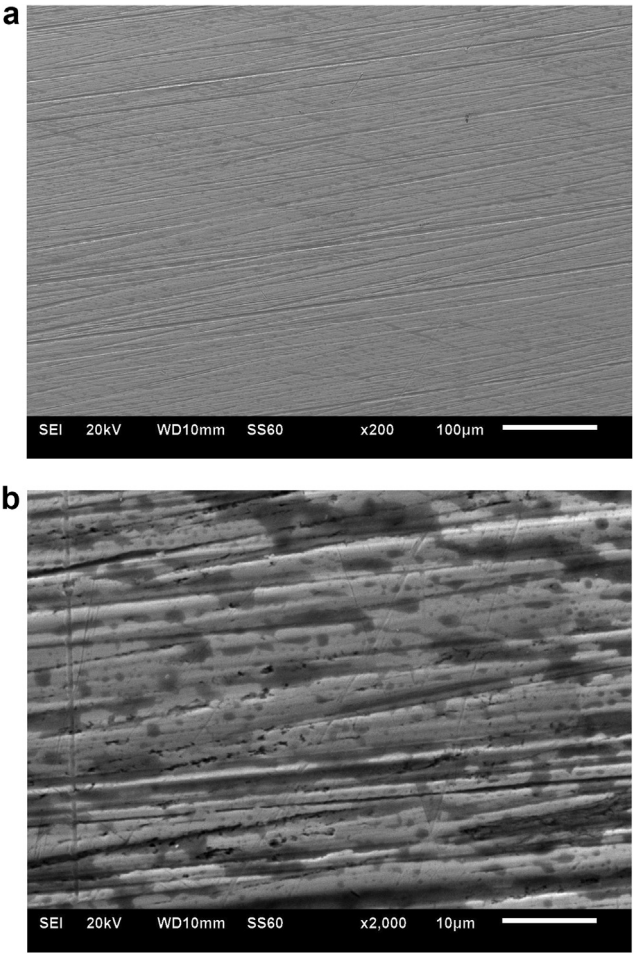

Fig. 6. Morphological features by SEM with resolution of a) 100 µm and (b) 10 µm.

kamacite stability temperature is below 723 °C or 600 °C, and at low pressure (Goldstein and Goddard, 1965). Furthermore, note that the kamacite is found only in meteorite. This was discovered by the Mars Exploration Rover (MER).

Additionally, the carbonate mineral (dolomite) is yellowish to brown in color; it is the secondary mineral formed by biotic activity, elucidated in Fig. 5. It occurred where the more highly altered meteorite was noticed (Scott, 1997), perhaps reflecting the greater temperature in the meteorite parent body at this location. Scoot (Scott, 1997) proposed a carbonate origin as the secondary mineral formed at high temperatures (more than 650 °C) due to the melts produced during a large impact on Mars 4.0 billion years ago. Likewise, the carbonate initiated by the reaction between silicates and the fluid rich in carbon dioxide infiltrated the fractured rock at depth during the impacted event.

Fig. 7 shows a plot of Ge and Ga versus Ni concentration. The studied area is represented and located in the IIC meteorite subgroup of the IIAB group. Therefore, the studied meteorite is classified as iron-nickel known as meteoric iron, and the IIC type is connected to the IIAB iron meteorite group (McSween, 1987). It overwhelmingly consists of iron-nickel, which usually consists of the mineral's phases: kamacite, taenite, and carbonatite originating from the cores of planetesimals (Weisberg et al., 2006).

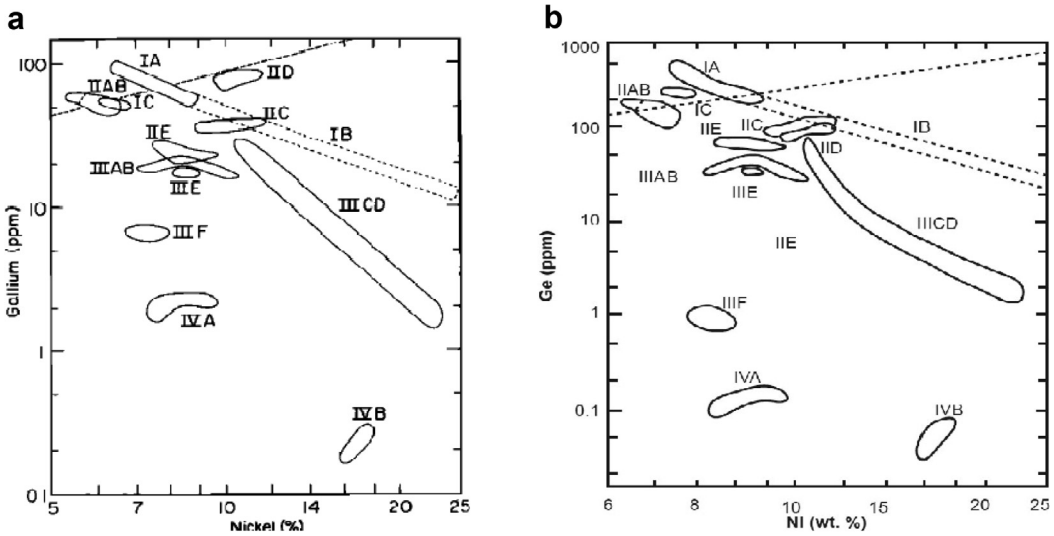

Fig. 7. Plot of Ge and Ga versus Ni for the studied meteorite, which is genetically quite similar to IIC subgroup or IIAB group.

Table 4
Summary of Ni, Ge, and Ga concentrations of Al Khamasain meteorite.

Meteorite	Ni %	Ga	Ge
Al Khamasain	9	37	85

3.5. Classification of the studied meteorites

Recently, a new classification scheme for meteorites proposed by Weisberg et al. (2006) subdivided all meteorites into two main groups, chondrites (undifferentiated meteorite) containing chondrules and primitive achondrites (non-chondritic meteorites), which are considered igneously differentiated, as shown in Fig. 8, evidently based on their bulk compositions and textures.

Moreover, the structural parameters can be combined with the meteorite chemical classification based on the concentration of the trace elements. These elements are germanium (Ge) and Gallium (Ga) (Lovering et al., 1957). Later, Wasson and Scott (1975) comprehended that the two elements, Ge and Ga, could not classify all the iron meteorites. Nevertheless, it is believed that the elements Ga and Ge remain the best taxonomic parameters because of their narrow ranges within groups. On the other hand, the nickel concentration should be specific to generate a classification scheme for producing a distinct discrimination of the parent iron meteorite. The low concentration of nickel in the studied meteorite, ranging from 5 to 9% would have an influence on the mineral fractionation from taenite to kamacite during the meteorite's cooling. The concentrations of Ni, Ga, and Ge for the studied meteorite were 9%, 37 ppm, and 85 ppm, respectively. Therefore, the lower the Ni concentration, the more kamacite minerals are formed. From all these considerations we may put the present meteorite in the subgroups of IIB, IIA, and IIC (Fig. 7).

4. Conclusion

This paper is a preliminary study, presenting some interesting insights about the nature of the biggest meteorite of KSA.

It is essentially an Fe-Ni-Co type alloy formed during planetary system evolution. From the composition, it is very likely that it was roaming in the asteroid belt between Mars and Jupiter, as no other belts or planets have such iron-rich rocks. Also, it is very unlikely to be of lunar origin, since moon meteorites, i.e., lunaite, have different composition; the composition of this KSA meteorite is very different than any lunar samples obtained from manned missions.

Our study has also shown that the XRF is best for determining elemental composition, though LIBS is the only technique suited for remote sensing, with accuracy comparable to XRF.

This could be one of the very few papers with such detailed physical characterization of a meteorite employing sophisticated analytical instruments. As the objective of this paper is to give a perspective of the broad features of the material properties of the meteorite, it is only qualitative and not quantitative.

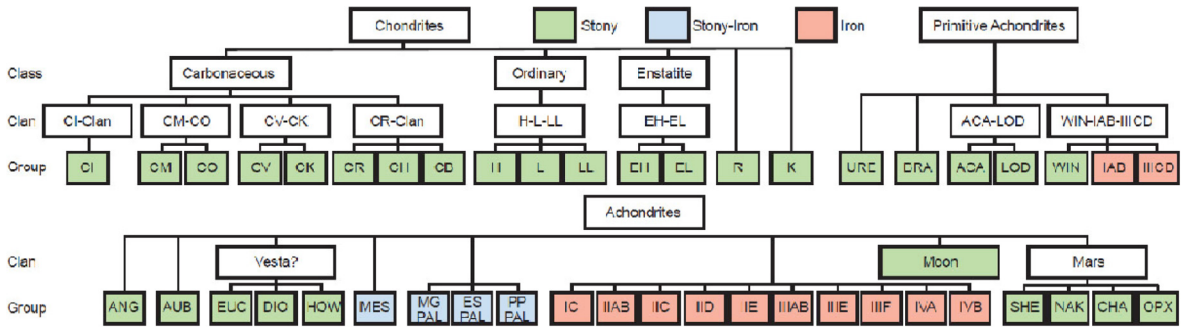

Fig. 8. Meteorite breaks along the crystal planes as bands.

Declaration of Competing Interest

The authors declare that they have no known competing financial interests or personal relationships that could have appeared to influence the work reported in this paper.

Acknowledgements

The authors are grateful to the Deanship of Scientific Research, King Saud University for funding through Vice Deanship of Scientific Research Chairs.

References

Abedin, K.M., Haider, A.F.M.Y., Rony, M.A., Khan, Z.H., 2011. Identification of multiple rare earths and associated elements in raw monazite sands by laser-induced breakdown spectroscopy. Opt. Laser Technol. 43 (1), 45–49. https://doi.org/10.1016/j.optlastec.2010.05.003.

Clegg, S.M., Sklute, E., Dyar, M.D., Barefield, J.E., Wiens, R.C., 2009. Multivariate analysis of remote laser-induced breakdown spectroscopy spectra using partial least squares, principal component analysis, and related techniques. Spectrochim. Acta Part B-Atomic Spectrosc. 64 (1), 79–88. https://doi.org/10.1016/j.sab.2008.10.045.

Corrigan, C.M., Chabot, N.L., McCoy, T.J., McDonough, W.F., Watson, H.C., Saslow, S. A., Ash, R.D., 2009. The iron-nickel-phosphorus system: effects on the distribution of trace elements during the evolution of iron meteorites. Geochim. Cosmochim. Acta 73 (9), 2674–2691. https://doi.org/10.1016/j.gca.2008.11.045.

Cremers, D.A., Radziemski, L.J., 2006. Handbook of laser-induced breakdown spectroscopy. Handbook of Laser-induced Breakdown Spectroscopy. https://doi.org/10.1002/0470093013.

De Giacomo, A., Dell'Aglio, M., De Pascale, O., Longo, S., Capitelli, M., 2007. Laser induced breakdown spectroscopy on meteorites. Spectrochim. Acta - Part B At. Spectrosc. 62 (12), 1606–1611. https://doi.org/10.1016/j.sab.2007.10.004.

Dequaire, T., Meslin, P.Y., Beck, P., Jaber, M., Cousin, A., Rapin, W., Lasne, J., Gasnault, O., Maurice, S., Buch, A., Szopa, C., Coll, P., 2017. Analysis of carbon and nitrogen signatures with laser-induced breakdown spectroscopy; the quest for organics under Mars-like conditions. Spectrochim. Acta - Part B At. Spectrosc. 131, 8–17. https://doi.org/10.1016/j.sab.2017.02.015.

Farooq, W.A., Al-Mutairi, F.N., Alahmed, Z.A., 2013. Analysis of rocks around capital of Kingdom of Saudi Arabia using laser induced breakdown spectroscopy. Opt. Spectrosc. 115 (2), 241–248. https://doi.org/10.1134/S0030400X13080079.

Farooq, W.A., Al-Mutairi, F.N., Khater, A.E.M., Al-Dwayyan, A.S., AlSalhi, M.S., Atif, M., 2012. Elemental analysis of fertilizer using laser induced breakdown spectroscopy. Opt. Spectrosc. (English Transl. Opt. i Spektrosk. 112 (6), 874–880. https://doi.org/10.1134/S0030400X12060082.

Farooq, W.A., Atif, M., Tawfik, W., Alsalhi, M.S., Alahmed, Z.A., Sarfraz, M., Singh, J.P., 2014. Study of bacterial samples using laser induced breakdown spectroscopy. Plasma Sci. Technol. 16 (12), 1141–1146. https://doi.org/10.1088/1009-0630/16/12/10.

Goldstein, J.I., Goddard, 1965. The formation of the Kamacite phase in metallic meteorites. J. Geophys. Res. 70, 6223–6232.

Hahn, David W., Omenetto, Nicoló, 2012. Laser Induced Breakdown Spectroscopy (LIBS), Part II: review of instrumental and methodological approaches to material analysis and applications to different fields. Appl. Spectrosc. 66 (4), 347–419. https://doi.org/10.1366/11-06574.

Harmon, R.S., Russo, R.E., Hark, R.R., 2013. Applications of laser-induced breakdown spectroscopy for geochemical and environmental analysis: a comprehensive review. Spectrochim. Acta - Part B At. Spectrosc. 10.1016/j.sab.2013.05.017

Harry Y. McSween, J.R., 1987. Meteorite and their parent Plants. The Press Syndicate of the University of Cambridge The.

Hebbert, H.U., 1955. Contribution of metallurgy to the origin of m&mites Part II-The signibuee of Nenmann bands in meteorites. ~~et~ormochimlcr. Act 7, 1.34 to 42.

Scott, Edward R.D., Wasson, John T., 1975. Classification and properties of iron meteorites. Geophys. Sp. Phys. 13 (4), 527. https://doi.org/10.1029/RG013i004p00527.

Lovering, J.F., Walter N., A., H.B., 1957. The Distribution of gallium, germanium, cobalt, chromium, and copper in iron and stony-iron meteoritea in relation to nickel content and structure. Geochim. Cosmochim. Aeta II, 263–278.

Lpsc xlviii , 2017. 286, 1238670. 10.1126/science.1238670.

Masilamani, V., Alarif, N., Farooq, W.A., Atif, M., Ramay, S., Althobaiti, H.S., Anwar, S., Elkhedr, I., AlSalhi, M.S., Abuamarah, B.A., 2019. Physical Characteristics of the Massive Meteorite of Saudi Empty Quarter. https://doi.org/10.1007/978-3-030-01575-6_18.

Norton, O.R., 1994. Rocks from Space Meteorite and Meteorite Hunters. Mountain Press Publishing Company, Missoula, Montana 59806.

Ramakrishnaiah, R., Farooq, W.A., Al Kheraif, A.-A.A., Qasim, S.B., Aldwayyan, A.S., 2012. Laser induced breakdown spectroscopic analysis of dental elastomeric impression materials. Middle East. J. Sci. Res. 11.

Sarfraz, Mansoor, Farooq, W A, Al-Eshaikh, Mohammad A, Kadachi, Ahmed N, Aldwayyan, A S, Ahmad, Kaleem, 2013. Analysis of allyl diglycol carbonate by laser induced-breakdown spectroscopy. Laser Phys. 23 (5), 055701. https://doi.org/10.1088/1054-660X/23/5/055701.

Scott, E.R.D., 1997. Shocked Carbonates May Spell in Martian Meteorite ALH84001 1–5.

Senesi, Giorgio S., 2014. Laser-Induced Breakdown Spectroscopy (LIBS) applied to terrestrial and extraterrestrial analogue geomaterials with emphasis to minerals and rocks. Earth-Sci. Rev. 139, 231–267. https://doi.org/10.1016/j.earscirev.2014.09.008.

Senesi, Giorgio S., Tempesta, Gioacchino, Manzari, Paola, Agrosì, Giovanna, 2016. An innovative approach to meteorite analysis by laser-induced breakdown spectroscopy. Geostand. Geoanal. Res. 40 (4), 533–541. https://doi.org/10.1111/ggr.2016.40.issue-410.1111/ggr.12126.

Sturm, V., Noll, R., 2003. Laser-induced breakdown spectroscopy of gas mixtures of air, CO2, N-2, and C3H8 for simultaneous C, H, O, and N measurement. Appl. Opt. 42, 6221–6225.

Tawfik, W., Bousiakou, L.G., Qindeel, R., Farooq, W.A., Alonizan, N.H., Fatani, A.J., 2015. Trace analysis of heavy metals in groundwater samples using laser induced breakdown spectroscopy (LIBS). Optoelectron. Adv. Mater. Rapid Commun. 9, 185–192.

Tawfik, W., Farooq, W.A., Alahmed, Z.A., Sarfraz, M.M., Ahmad, K., Yakuphanoglu, F., 2013. Characterization and analysis of nanostructured CdO thin film using LIBS technique. In: 2013 Saudi International Electronics, Communications and Photonics Conference, SIECPC, 2013. 10.1109/SIECPC.2013.6550798

Tempesta, Gioacchino, Agrosì, Giovanna, 2016. Standardless, minimally destructive chemical analysis of red beryls by means of Laser Induced Breakdown Spectroscopy. Eur. J. Mineral. 28 (3), 571–580. https://doi.org/10.1127/ejm/2016/0028-2529.

Weisberg, M.K., McCoy, T.J., Krot, A.N., 2006. Systematics and evaluation of meteorite classification. Meteorites Early Sol. Syst. II, 19–52.